Hindawi
Mathematical Problems in Engineering
Volume 2019, Article ID 8912341, 11 pages
https://doi.org/10.1155/2019/8912341

Research Article

Error Mechanism and Self-Calibration of Single-Axis Rotational Inertial Navigation System

Bo Nie, Guiming Chen, Xianting Luo, and Bingqi Liu

High-Tech Institute of Xi'an, Xi'an 710025, China

Correspondence should be addressed to Bingqi Liu; iqgnibuil@126.com

Received 19 January 2019; Revised 28 May 2019; Accepted 6 September 2019; Published 30 September 2019

Academic Editor: Luis M. López-Ochoa

With the rapid development of inertial technology, the rotational inertial system has been widely used for high-accuracy navigation. In addition, the single-axis rotational inertial navigation system is one of the most popular navigation systems due to its low cost. However, the fact which cannot be ignored is that although single axis rotational inertial navigation system can restrain divergence of attitude error, it cannot eliminate velocity error, which is mainly caused by the gyro misalignment and scale factor error related to rotational axis. A novel calibration method established on filter has been proposed. Position, velocity, and attitude are chosen to be the state variables. In order to estimate the gyro errors related to rotational axis, these errors must be included in the state equation. Correspondingly, zero velocity and rate of turntable are chosen to be measured. Simulation has been carried out to verify the correctness of the theory, and the real test has been performed to further demonstrate the validity of the method. By compensating the main error estimated by filter, it can be found that the accumulated errors in velocity and attitude are decreased. So, the precision of navigation is greatly improved with the proposed method.

1. Introduction

Inertial navigation system (INS) can obtain position, attitude, and velocity of the craft by resolving the data sampled by its inertial measurement unit, which is IMU and contains three orthogonal gyros and accelerometers [1]. Thus, the INS is self-contained and widely used in military field such as airplanes, submarines, and ships. INS can be divided into two categories: platform and strap-down inertial navigation system. Compared with platform INS, strap-down INS has the characteristics of higher reliability, smaller volume, better maintenance, and lower cost [2–4].

Device error is affected by the precision of the navigation. Meanwhile, velocity and attitude errors will accumulate with time quickly [5]. There are two major approaches to enhance the precision of inertial navigation. One is to improve the performance of gyro and accelerometer. However, this method is expensive and restricted by technique. The other one is error compensation. Compensation can be performed based on the external information such as Global Positioning System (GPS) and turntable [6]. Self-compensation is another way to eliminate the device error. Rotation modulation technology has been one of the most widely used self-compensation methods, especially in the field of aerospace for its low cost and reliability.

In rotational inertial navigation system (RINS), IMU is placed on the indexing mechanization which is fixed on the craft [7–9]. Thus, the self-compensation can be performed by designing appropriate rotating sequence. RINS can be divided into single-axis, dual-axis, and triaxial-axis or above [10–12].

The advantage of rotation modulation is that it can realize self-compensation of sensor errors during navigation process [13, 14]. However, errors still exist and affect the precision of the navigation.

In triaxis RINS, instrument errors, such as accelerometer nonlinearity and inner lever-arm, can be accurately compensated through optimal estimation with velocity and position error measurements. Meanwhile, proper rotation scheme design can help modulate and estimate error

parameters of IMU. Taking commercial cost into consideration, triaxis and dual-axis RINSs are more expensive than single-axis [15–18]. In consequence, single-axis RINS will be mainly discussed in this paper.

In single-axis RINS, gyro drift is the main concern. Shang et al. [19] pointed out that single-axis rotation can modulate the constant drift perpendicular to the rotational axis, while gyro drift on the spin axis still diverge with time. In order to deal with the constant drift of spin axis, identification methods of gyro drift have been proposed. Yu et al. [20] calibrated the single-axis gyro drift by using radial basis function network. A least square method was established to calibrate the axial gyro drift precisely by Hu et al. [21]. Similar methods of calibration of gyro drifts are shown in [22–24].

Besides the gyro drift, error propagation of the single axis rotational INS showed that scale factor error and misalignment errors related to the rotational axis cannot be modulated [25, 26]. The scale factor error along the rotational axis was the main error that affected the single-axis rotational INS in [27]. However, no paper can give answer to this question. Therefore, a novel method which can calibrate the instrument errors is proposed in this article.

Compared with other methods, the method proposed in this paper is suitable for single-axis RINS to calibrate main device errors by using zero velocity and attitude errors. Thus, compensation can be made to reduce the error accumulation during the navigation process. Based on this, the precision of the single-axis RINS can be promoted.

The advantages of the proposed method are shown as follows: according to single-axis rotational inertial navigation system, this paper provides the deduction of error propagation in terms of misalignment and scale factor error related to rotational axis. Besides, it points out that in single-axis RINS, attitude error caused by gyro misalignment related to rotational axis can be modulated, but velocity error still exists. Simulation has been carried out to verify this thesis. By observing the velocity and rate of turntable, gyro misalignment and scale factor errors of the rotational axis can be estimated under stationary base.

The paper is organized as follows. Section 2 provides the error mechanism of single axis rotational INS. Section 3 introduces the design of filter for single-axis rotational system. Section 4 describes the process of the simulation, which is carried out to verify the error mechanism and the proposed method. In order to further demonstrate the proposed method, experiment has been performed and results are shown in Section 5. Conclusion is drawn in Section 6.

2. Error Mechanism

The denotation of frames is shown in Figure 1, where i denotes earth-centered inertial frame, e denotes earth-centered frame, n denotes navigation frame, and b denotes body frame.

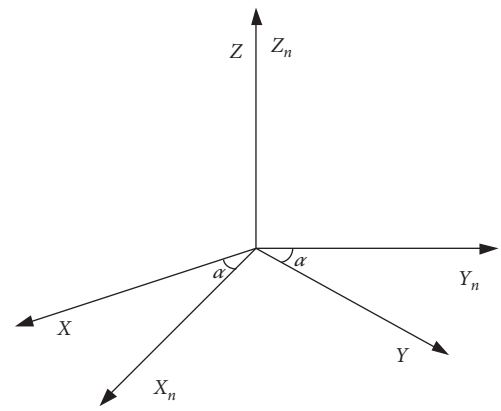

Figure 1: Wander azimuth frame.

2.1. Wander Azimuth Frame. The wander frame is widely used in navigation system, and it can be obtained by rotating with respect to the local geodetic frame z axis by the wander frame angle α.

In this paper, considering the fact calibration is performed on stationary base, α is chosen to be zero. The error model in local geodetic frame can be considered the same as wander azimuth frame in a short time.

2.2. Error Analysis. To further demonstrate the error mechanism in this paper, simplification and assumption are given.

The IMU can be rotated about the vertical body axis with constant angular velocity ω:

$$\delta\omega_{ib}^{b} = \widetilde{\omega}_{ib}^{b} - \omega_{ib}^{b} = \begin{bmatrix} gB_x \\ gB_y \\ gB_z \end{bmatrix} + \begin{bmatrix} S_x & M_{xy} & M_{xz} \\ M_{yx} & S_y & M_{yz} \\ M_{zx} & M_{zy} & S_z \end{bmatrix} \begin{bmatrix} \omega_{ibx}^{b} \\ \omega_{iby}^{b} \\ \omega_{ibz}^{b} \end{bmatrix}. \tag{1}$$

The gyro angular velocity error equation is shown above, where $\widetilde{\omega}_{ib}^{b}$ denotes the measured angular velocity in the body frame, ω_{ib}^{b} denotes the true angular velocity, $\delta\omega_{ib}^{b}$ denotes the angular velocity error, gB_i denotes gyro bias, S_i denotes the scale factor error, and M_{ij} denotes the misalignment:

$$\begin{aligned} \omega_{eb}^{b} &= \begin{bmatrix} 0 & 0 & \omega \end{bmatrix}^{T}, \\ \omega_{ib}^{b} &= \omega_{ie}^{b} + \omega_{eb}^{b}, \end{aligned} \tag{2}$$

where ω_{eb}^{b} denotes the angular velocity provided by turntable, which rotates around the body spin axis with constant rate ω and ω_{ie}^{b} denotes the earth angular velocity in the body frame.

Gyro error model is given by equation (1). Considering the angular velocity provided by turntable is much larger than the earth angular velocity and gyro bias, the approximation of gyro model is shown as follows:

$$\begin{aligned}\delta\omega_{ib}^{b} &\approx \begin{bmatrix} S_x & M_{xy} & M_{xz} \\ M_{yx} & S_y & M_{yz} \\ M_{zx} & M_{zy} & S_z \end{bmatrix} \begin{bmatrix} \omega_{iex}^{b} \\ \omega_{iey}^{b} \\ \omega_{iez}^{b} + \omega \end{bmatrix} \\ &\approx \begin{bmatrix} S_x & M_{xy} & M_{xz} \\ M_{yx} & S_y & M_{yz} \\ M_{zx} & M_{zy} & S_z \end{bmatrix} \begin{bmatrix} 0 \\ 0 \\ \omega \end{bmatrix} \\ &= \omega \cdot \begin{bmatrix} M_{xz} \\ M_{yz} \\ S_z \end{bmatrix}. \end{aligned} \tag{3}$$

The simplified gyro error model shows that the most important error sources are M_{xz}, M_{yz}, S_z. Correspondingly, the velocity error accumulated by inertial device error will directly affect the precision of navigation. The rotation sequence from navigation frame to body frame is yaw, pitch, and roll, respectively:

$$C_b^n = C_s^n \cdot C_b^s, \tag{4}$$

$$\begin{aligned} C_s^n &= \begin{bmatrix} \cos\gamma_0 \cos\varphi_{G0} - \sin\gamma_0 \sin\theta_0 \sin\varphi_{G0} & -\cos\theta_0 \sin\varphi_{G0} & \sin\gamma_0 \cos\varphi_{G0} + \cos\gamma_0 \sin\theta_0 \sin\varphi_{G0} \\ \cos\gamma_0 \sin\varphi_{G0} + \sin\gamma_0 \sin\theta_0 \cos\varphi_{G0} & \cos\theta_0 \cos\varphi_{G0} & \sin\gamma_0 \sin\varphi_{G0} - \cos\gamma_0 \sin\theta_0 \cos\varphi_{G0} \\ -\sin\gamma_0 \cos\theta_0 & \sin\theta_0 & \cos\gamma_0 \cos\theta_0 \end{bmatrix}, \\ C_b^s &= \begin{bmatrix} \cos\zeta & -\sin\zeta & 0 \\ \sin\zeta & \cos\zeta & 0 \\ 0 & 0 & 1 \end{bmatrix}, \end{aligned} \tag{5}$$

where C_b^s is the direction cosine matrix of body frame, C_s^n is used to transfer the initial body frame to the wander azimuth navigation frame, φ_{G0} denotes the initial yaw angle, γ_0 denotes the initial roll angle,, θ_0 denotes the initial pitch angle, and ζ denotes rotation angle around spin axis from initial frame s to body frame b.

The attitude error can be defined as (concrete deduction is shown in Appendix)

$$\begin{aligned}\phi(t) &= \phi(0) + \delta\phi(t) \\ &= \phi(0) + C_s^n \begin{bmatrix} M_{xz}\sin\omega t + M_{yz}\cos\omega t - M_{yz} \\ -M_{xz}\cos\omega t + M_{yz}\sin\omega t + M_{xz} \\ S_z\omega t \end{bmatrix}, \end{aligned} \tag{6}$$

where $\phi(0)$ denotes the attitude error at the beginning and $\delta\phi(t)$ denotes the accumulated attitude error. From equation (6), it can be seen that the accumulated leveling attitude error can be modulated by 2π rotation. However, the initial attitude error $\phi(0)$ still exists and has great effect on the velocity error.

Besides, scale factor error of the rotational axis gyro will affect yaw angle. The velocity error dynamic equations demonstrate the relationship between attitude error and velocity error as follows:

$$\begin{aligned}\delta\dot{v}_x &= \delta f_x - g\phi_y, \\ \delta\dot{v}_y &= \delta f_y + g\phi_x, \end{aligned} \tag{7}$$

Velocity errors can be obtained by the integral of equation (7). To research the factors that affect velocity, expansion of integral is shown as follows (concrete deduction is given in Appendix):

$$\begin{aligned}\delta v_x(t) &= \delta v_x(0) + \int_0^t \left(\delta f_x - g\phi_y\right)dt \\ &= \Bigg(\delta v_x(0) - C_s^n(2,1)\frac{g}{\omega}\Big(-M_{xz}\cos\omega t \\ &\quad + M_{yz}\sin\omega t + M_{xz}\Big) + C_s^n(2,2)\frac{g}{\omega}\Big(M_{xz}\sin\omega t \\ &\quad + M_{yz}\cos\omega t - M_{yz}\Big)\Bigg) + \Big(-g\phi_y(0)t \\ &\quad + C_s^n(2,1)gM_{yz}t - C_s^n(2,2)gM_{xz}t \\ &\quad - C_s^n(2,3)\frac{g}{2}S_z\omega t^2\Big). \end{aligned} \tag{8}$$

From the final expansion of equation (8), it can be seen that terms in the first bracket are converged because trigonometric function is bounded. Terms in the second bracket are diverging with time. Thus, the drift of velocity $\delta v_x(t)$ is mainly caused by the items in the second bracket that contains initial attitude error, gyro misalignment, and scale factor error related to rotational axis.

Similarly, the error velocity $\delta v_y(t)$ can be expressed as

$$\begin{aligned}\delta v_y(t) &= \delta v_y(0) + \int_0^t \left(\delta f_y + g\phi_x\right)dt \\ &= \left(\delta v_y(0) + C_s^n(1,1)\frac{g}{\omega}\left(-M_{xz}\cos\omega t + M_{yz}\sin\omega t + M_{xz}\right) - C_s^n(1,2)\frac{g}{\omega}\left(M_{xz}\sin\omega t + M_{yz}\cos\omega t - M_{yz}\right)\right) \\ &\quad + \left(g\phi_x(0)t - C_s^n(1,1)gM_{yz}t + C_s^n(1,2)gM_{xz}t + C_s^n(1,3)\frac{g}{2}S_z\omega t^2\right).\end{aligned} \tag{9}$$

Obviously, the main angular velocity error above, which is induced by scale factor error and misalignment error related to body spin axis, cannot be modulated during the rotation. The navigation attitude error will accumulate quickly because of this. Thus, the precision of the INS navigation system can be improved by using the self-calibration method to estimate the errors related to body spin axis.

3. Design of Filter for Single-Axis Rotational System

According to the error mechanism, the proposed method should estimate the instrument errors including scale factor errors and misalignment of the related rotation axis. Besides, the navigation information, position, velocity, and attitude should also be contained in the measurement matrix. Correspondingly, the measurement model of the proposed method should be established by parameters that can be obtained precisely.

3.1. State Equation. The state model chosen in this paper is listed as follows:

$$X(t) = \left[\delta\theta_x \;\; \delta\theta_y \;\; \delta h \;\; \delta v_x \;\; \delta v_y \;\; \delta v_z \;\; \psi_x \;\; \psi_y \;\; \psi_z \;\; M_{xz} \;\; M_{yz} \;\; S_z\right]^T, \tag{10}$$

where $\delta\theta_x$, $\delta\theta_y$, and δh denote position errors, δv_x, δv_y, and δv_z denote velocity errors, ψ_x, ψ_y, and ψ_z denote attitude errors, and M_{xz}, M_{yz}, and S_z denote deterministic unknown errors.

(1) Instrument error equations

The gyro errors are modelled as constant during the filtering process:

$$\begin{cases} \dot{M}_{xz} = 0, \\ \dot{M}_{yz} = 0, \\ \dot{S}_z = 0. \end{cases} \tag{11}$$

(2) Attitude error equations:

$$\begin{cases} \dot{\psi}_x = \omega_z\psi_y - \omega_y\psi_z - \varepsilon_x', \\ \dot{\psi}_y = -\omega_z\psi_x + \omega_x\psi_z - \varepsilon_y', \\ \dot{\psi}_z = \omega_y\psi_x - \omega_x\psi_y - \varepsilon_z', \\ \omega = \rho + \Omega, \end{cases} \tag{12}$$

where $\dot{\psi}_i$ denotes dynamic error, ε_i' denotes gyro error under navigation system, ρ denotes the navigation to earth frame angular rotation rate in the navigation frame, and Ω denotes the Earth's rotation rate.

(3) Velocity error equations:

$$\begin{cases} \delta\dot{v}_x = -g\delta\theta_y + 2\Omega_z\delta v_y - (\rho + 2\Omega)_y v_z - f_z\psi_y + f_y\psi_z + \nabla_x, \\ \delta\dot{v}_y = g\delta\theta_x - 2\Omega_z\delta v_x - (\rho + 2\Omega)_x v_z + f_z\psi_x - f_x\psi_z + \nabla_y, \\ \delta\dot{v}_z = 2\frac{g}{R}\delta h + \left(\omega_y + \Omega_y\right)\delta v_x - \left(\omega_x + \Omega_x\right)\delta v_y - f_y\psi_x \\ \qquad + f_x\psi_y + \nabla_z, \end{cases} \tag{13}$$

where f_i denotes the sensed output of i-axis accelerometer, $\delta\theta_x$ and $\delta\theta_y$ denote the angular position errors, δh denotes the altitude error, and ∇_i denotes the error of accelerometer.

(4) Position error equations:

$$\begin{cases} \delta\dot{\theta}_x = -\frac{v_z}{R}\delta\theta_x - \frac{1}{R}\delta v_y, \\ \delta\dot{\theta}_y = -\frac{v_z}{R}\delta\theta_y + \frac{1}{R}\delta v_x, \\ \delta\dot{h} = \delta v_z, \end{cases} \tag{14}$$

where R denotes the earth radius.

(5) Gyro error model:

$$\begin{bmatrix}\varepsilon_x \\ \varepsilon_y \\ \varepsilon_z\end{bmatrix}^n = C_b^n\left(\begin{bmatrix}B_x \\ B_y \\ B_z\end{bmatrix} + \begin{bmatrix}S_x & M_{xy} & M_{xz} \\ M_{yx} & S_y & M_{yz} \\ M_{zx} & M_{zy} & S_z\end{bmatrix}\cdot\begin{bmatrix}\omega_{ib}^x \\ \omega_{ib}^y \\ \omega_{ib}^z\end{bmatrix}\right), \tag{15}$$

where ε_i denotes the angular velocity error caused by gyro, B_i denotes the bias of i-axis gyro, S_i denotes the scale factor error of i-axis gyro, and M_{ij} denotes the misalignment error of gyro in i-axis related to j-axis.

3.2. Measurement Model. The angular velocity provided by rate turntable is much larger than that of the earth, so the

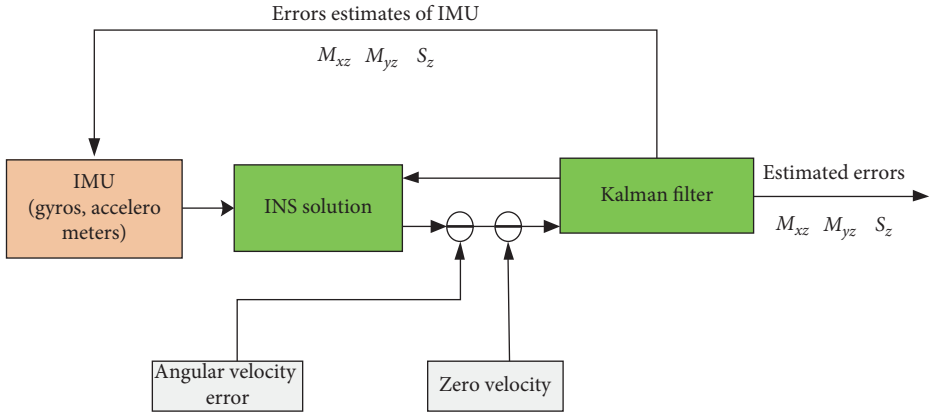

Figure 2: Flow chart of self-calibration filter in the proposed method.

errors are mainly caused by scale factor errors and misalignment errors related to rotational axis. Thus, the error of gyro output and the velocity during navigation process can be utilized as observations to estimate the corresponding errors.

(1) Given that the IMU is tested on stationary base, the velocity of IMU should be zero. The output velocity of IMU can be defined as the measurement Z_1:

$$Z_1 = \delta V = V_{\text{ins}} - 0 = \begin{bmatrix} \delta v_x \\ \delta v_y \\ \delta v_z \end{bmatrix}. \tag{16}$$

The measurement equation of sensed velocity of tested IMU can be described as

$$Z_1(t) = H_1 X(t) + \eta, \tag{17}$$

where the measurement matrix is

$$H_1 = \begin{bmatrix} 0_{1\times3} & 1 & 0 & 0 & 0_{1\times6} \\ 0_{1\times3} & 0 & 1 & 0 & 0_{1\times6} \\ 0_{1\times3} & 0 & 0 & 1 & 0_{1\times6} \end{bmatrix}. \tag{18}$$

(2) The attitude error always exists and the computed attitude matrix translating from navigation frame to body frame is represented as

$$\tilde{C}_n^b = (I - \phi\times)C_n^b, \tag{19}$$

where ϕ denotes tilt error and C_n^b denotes attitude direction cosine matrix without attitude error. The input rate of turntable and the rate of earth rotation can be considered as references, and the output rate of IMU can be measured by gyros. Thus, the measurement Z_2 is defined to be the difference between the measured angular velocity and the true angular velocity:

$$\begin{aligned} Z_2 &= \delta\omega_{ib}^b = \tilde{\omega}_{ib}^b - \tilde{C}_n^b\omega_{ie}^n - \tilde{\omega}_{eb}^b, \\ &= \delta\tilde{\omega}_{ib}^b + C_n^b(\omega_{ie}^n\times)\phi_n, \end{aligned} \tag{20}$$

and the measurement matrix of H_2 can be expressed as

$$H_2 = \begin{bmatrix} & \omega_{ibz}^b & 0 & 0 \\ 0_{3\times6} \quad C_n^b\times\omega_{ie}^n & 0 & \omega_{ibz}^b & 0 \\ & 0 & 0 & \omega_{ibz}^b \end{bmatrix}. \tag{21}$$

(3) Flow chart of self-calibration filtering is given in Figure 2.

The principle of the proposed calibration method in this paper to estimate the unknown errors is shown in Figure 2. Figure 2 uses angular velocity and zero velocity as the observed quantity. A 12-state Kalman filter is established by the INS dynamic equations and simplified gyro error model.

4. Simulation

To support the theory discussed above and evaluate the performance of the proposed method, simulations are carried out in Section 4.2.

4.1. Condition. The IMU errors in this simulation are defined as follows: gyro bias is 0.1°/h with a white noise of 0.01°/h/$\sqrt{\text{Hz}}$, accelerometers bias is 100 μg with a white noise of 10 μg/$\sqrt{\text{Hz}}$, misalignment of accelerometers is 20″, scale factor error of accelerometer is 100 ppm, the misalignment of gyro about rotational axis (z-axis of body frame) is 60″ and the others are 20″, and the scale factor error of gyro around rotation axis is 300 ppm and the others are 100 ppm. The main error parameters are listed in Table 1. Data sampling frequency is 50 Hz.

In order to validate the theory above, the initial attitude angles of roll, pitch, and yaw are 20°, 30°, and 40°, respectively. The tested IMU is under stationary base. The tested IMU rotates with the angular velocity of 10°/s, and the length of the test period t is 36 s.

4.2. Simulation Results. Assume that there is no attitude error at the beginning of navigation and the whole

Table 1: Main error sources of accelerators.

Bias (μg)			Misalignment (sec)						Scale factor error (ppm)			Noise (μg/$\sqrt{\text{Hz}}$)
∇_x	∇_y	∇_z	E_{xy}	E_{xz}	E_{yx}	E_{yz}	E_{zx}	E_{zy}	K_x	K_y	K_z	∇_n
100	100	100	20	20	20	20	20	20	100	100	100	30

Table 2: Main error sources of gyros.

Bias (°/h)			Misalignment (sec)						Scale factor error (ppm)			Noise (°/h/$\sqrt{\text{Hz}}$)
ε_x	ε_y	ε_z	M_{xy}	M_{xz}	M_{yx}	M_{yz}	M_{zx}	M_{zy}	S_x	S_y	S_z	ε_n
0.05	0.05	0.05	20	60	20	60	20	20	100	100	300	0.02

Table 3: Calibration result.

Parameter	M_{xz}	M_{yz}	S_z
Estimate	59.96	59.96	300.02

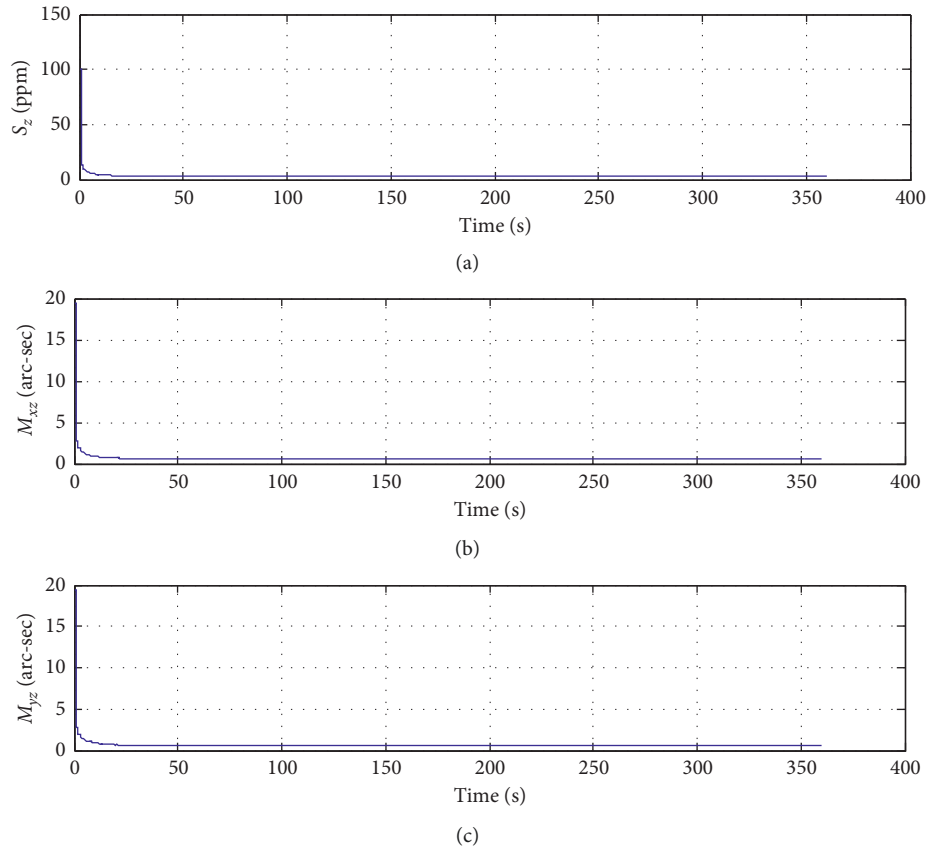

Figure 3: Error covariance root-mean-square curve of estimated device error.

navigation process lasts 360 s, including 10 whole periods t. Based on the error sources listed in Tables 1 and 2, the simulation results are evaluated by 30 Monte Carlos runs. The state variables of instrument errors are M_{xz}, M_{yz}, and S_z, and the values are 59.96″,59.96″, and 300 ppm, respectively. In Table 3, it is obvious that the estimated parameters obtained by 12-state filter are very close to the real values.

Figure 3 describes the error covariance root-mean-square curve of the state variables during the filtering process. The curve shows that the algorithm has better convergence speed, and the state variables M_{xz}, M_{yz}, and S_z have good observability.

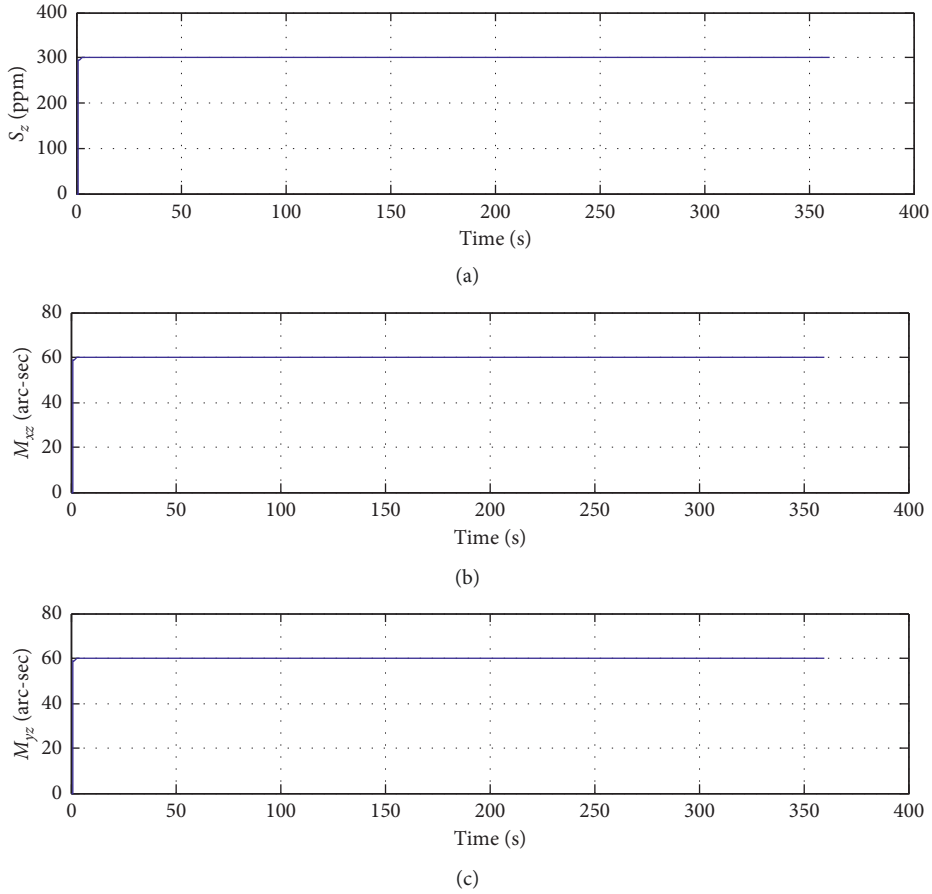

Figure 4: Estimation curve of device error related to rotational axis.

Figure 4 describes the estimated gyro scale factor errors and misalignment errors around rotational axis in 30 Monte Carlos runs. Similar to error covariance root-mean-square curve, error estimated curve also converges quickly after filtering. The steady values of estimated gyro scale factor errors and misalignment errors can be compensated during the navigation process. Navigation results after compensation are listed in Table 4.

Figure 5 describes the velocity error during navigation process without filter. The curve shows that velocity error accumulates with time quickly, which is the same as the unknown attitude error and the inertial device error related to rotational axis. Thus, the error mechanism deduction has been verified.

Table 4 provides a comparison of the navigation results under different conditions. Through 360 s navigation without compensation, the velocity errors V_x and V_y are 2.982 m/s and −17.548 m/s, and the attitude errors of roll, pitch, and yaw angles are 0.467°, 0.303°, and 0.911°. Meanwhile, Table 4 provides navigation results under the same condition after compensation. The velocity errors V_x and V_y are 0.065 and −0.024, and the attitude errors of roll pitch and yaw are −0.044°, 0.034°, and −0.092°, respectively.

Thus, simulation results show that velocity error caused by scale factor errors and misalignment errors related to rotation axis cannot be modulated by the single-axis rotational inertial navigation system. With the proposed method, the corresponding errors can be calibrated precisely. Simulation results show that navigation performance is greatly enhanced by calibration and compensation.

5. Real Test

5.1. Experiment Set up. To further validate the proposed method, the real calibration test is established. The test IMU consists of three orthogonal gyros whose accuracy is 0.1°/h and accelerometers whose accuracy is 100 μg. The test is carried out with personal computer made by DELL, industrial personal computer, the self-designed computer monitoring software, and navigation computing software.

Data are sampled by the frequency of 100 Hz. The turntable shown in Figure 6 is utilized to simulate single-axis rotational mechanization, whose rotation rate accuracy is 0.0001°/s. Besides, its positional accuracy is 2 arc-second. Initial angles of pitch, roll, and yaw are 0.0456°, 0.0279°, and 0.0197°. The rotation rate of turntable is 10°/s corresponding to the simulation.

In the beginning, the turntable remains stationary for 140 s to collect data for initial alignment. Then, the IMU rotates at the angular velocity of 10°/s around its z-axis at least 900 s for navigation. The turntable should be rotated to its original position after navigation.

Table 4: Pure navigation results.

Parameter	Before compensation	After compensation	Theory value
V_x (m/s)	2.982	0.0447	0
V_y (m/s)	17.548	0.1184	0
V_z (m/x)	0	0	0
Pitch (°)	20.467	19.954	20
Roll (°)	29.697	30.030	30
Yaw (°)	40.911	39.910	40

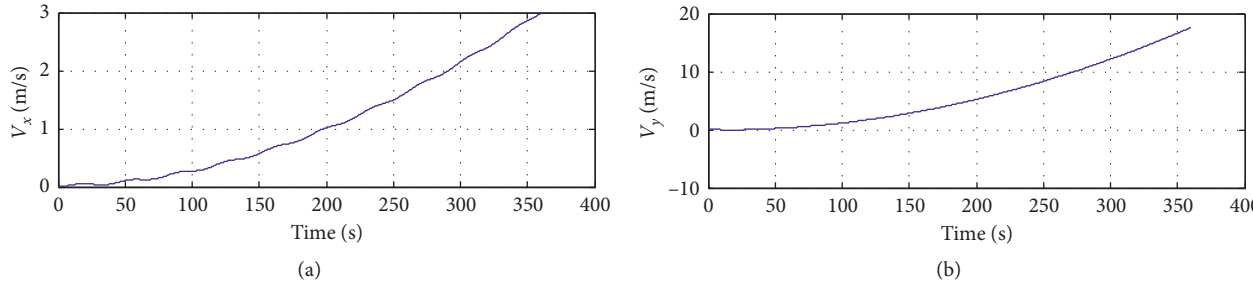

Figure 5: Velocity error curve resolved by single axis rotational INS without compensation.

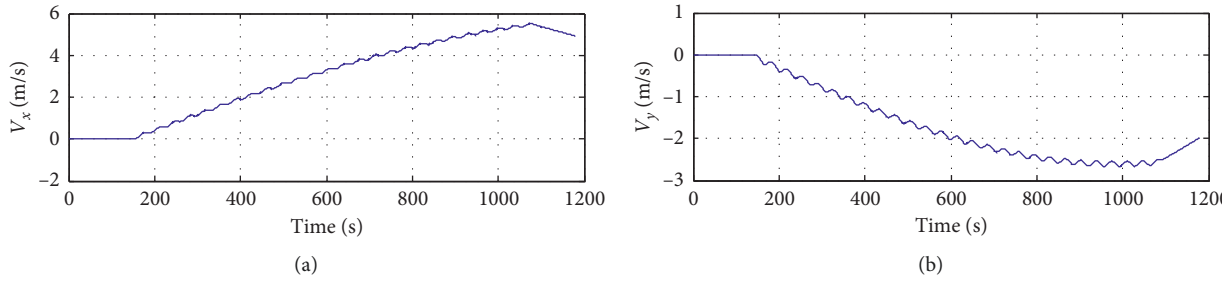

Figure 6: Velocity error of pure navigation before compensation.

Table 5: Calibration result.

Parameter	M_{xz}	M_{yz}	S_z
Estimated	154.2511	−107.7430	84.0126

5.2. Experiment Result. Gyro errors of rotation axis are estimated by the designed self-calibration filter. Estimated values of M_{xz}, M_{yz}, and S_z are shown in Figure 3. It is obvious that estimation curve converges very quickly. The steady values of estimated scale factor errors and misalignment errors M_{xz}, M_{yz}, and S_z related to rotational axis are utilized as calibration results. Calibration results estimated by filter are listed in Table 5, where M_{xz} is 154.2″, M_{yz} is −107.7″, and S_z is 84.0 ppm.

Figure 6 shows the navigation results of accumulated velocity errors before compensation. It is evident that velocity accumulates quickly, and it can be proved that single-axis rotational INS cannot modulate scale factor error and misalignment errors related to rotation axis. Figure 7 displays the velocity estimated curve after compensating for the corresponding errors. Compared with the estimated curve before compensation, the error accumulates more slowly. It proves that the proposed method can decrease or eliminate the effects caused by gyro in rotation axis. Figure 8 shows the V_x, V_y curve after compensation.

Navigation results about velocity and attitude are listed in Table 6. Before compensation, the velocity errors in level drift are 4.9222 m/s and −1.9773 m/s, respectively, while after compensation are 0.2950 m/s and 0.5888 m/s. In terms of attitude errors, the improvement after compensation is also obvious. Compared with the initial attitude, the attitude errors accumulated during navigation and resolved by single-axis rotational INS in pitch, roll, and yaw are 0.0426 degree, 0.1037 degree, and 0.8712 degree. Similarly, attitude errors in pitch, roll, and yaw angle after compensation are 0.0011 degree, 0.0834 degree, and 0.0771 degree. Data express that the precision of navigation is enhanced at least 20%.

Thus, the proposed method with filter can estimate the device error related to rotational axis effectively. The

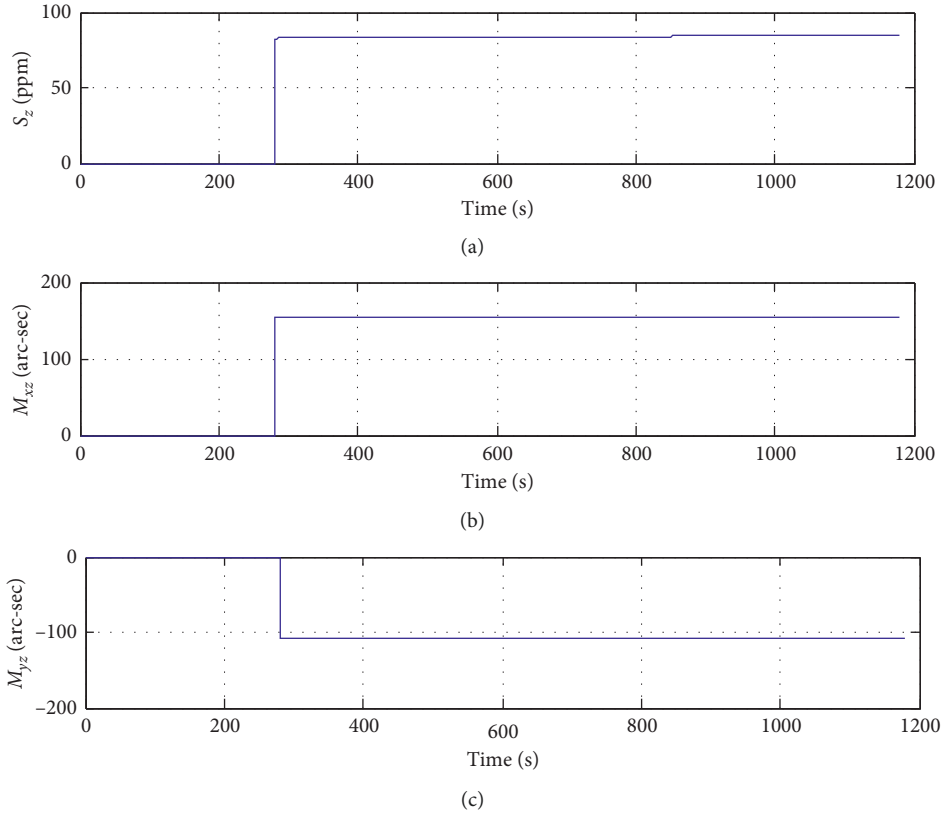

Figure 7: Errors estimation curve related to rotational axis gyro.

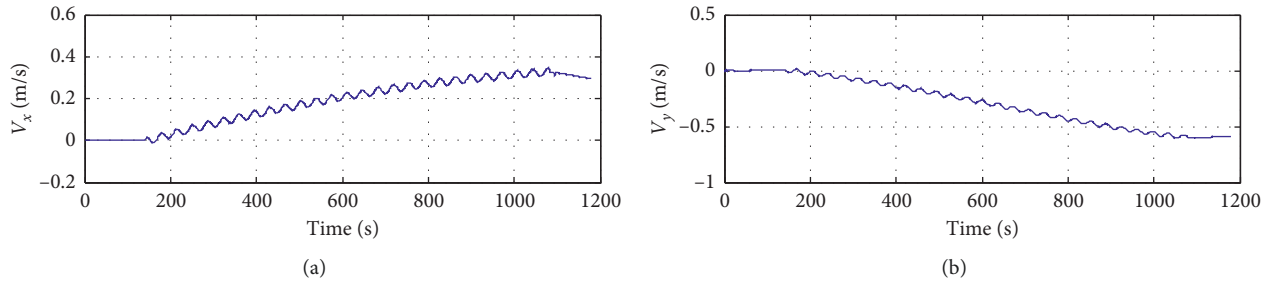

Figure 8: Velocity errors of pure navigation after compensation.

Table 6: Pure navigation results in experiment.

Parameter	Theory value	Before compensation	After compensation
V_x (m/s)	0	4.9222	0.2950
V_y (m/s)	0	−1.9773	0.5888
V_z (m/x)	0	0	0
Pitch (deg)	0.0456	0.0043	0.0467
Roll (deg)	0.0279	−0.0758	−0.0455
Yaw (deg)	0.0197	0.8809	0.0968

precision of the single axis rotational INS is improved by compensating the estimated steady value of corresponding errors.

6. Conclusions

In the single-axis rotational inertial navigation system, instrument errors related to rotational axis cannot be modulated and these errors will have great impact on the navigation precision. Error mechanism and equations of velocity and attitude have been shown in this paper, and a calibration method with filter has been proposed. The state model should contain device errors which cannot be modulated by rotation. In the stationary base, zero velocity and the known turntable angular velocity can be chosen as the measurement. IMU errors can be estimated and compensated online to reduce the navigation error. Simulation has been carried out to verify the correctness of error mechanism and the feasibility of the proposed method, the

experiment results further illustrate the validation of the proposed method, and the precision of the single-axis rotational INS can be improved.

It is shown that the precision of navigation is enhanced at least 20%. The proposed method using filter can estimate the device error related to rotational axis effectively. The precision of the single axis rotational INS has been improved by compensating the estimated steady value of corresponding errors.

Appendix

Deduction of equation (7):

$$\phi(t) = \phi(0) + \delta\phi(t). \tag{A.1}$$

In the equation, $\delta\phi(t)$ can be approximated as

$$\begin{aligned}\delta\phi(t) &= \int_0^t C_b^n \delta\omega_{ib}^b dt \\ &\approx \int_0^t C_b^n \begin{bmatrix} - & - & M_{xz} \\ - & - & M_{yz} \\ - & - & S_z \end{bmatrix} \begin{bmatrix} 0 \\ 0 \\ \omega \end{bmatrix} dt = \int_0^{\omega t} C_b^n \begin{bmatrix} M_{xz} \\ M_{yz} \\ S_z \end{bmatrix} d\varphi,\end{aligned} \tag{A.2}$$

where $\varphi = \omega t$, then inserting equation (5) into $\phi(t)$, we get

$$\begin{aligned}\phi(t) &= \phi(0) + \delta\phi(t) \\ &= \phi(0) + \int_0^{\omega t} C_b^n \begin{bmatrix} M_{xz} \\ M_{yz} \\ S_z \end{bmatrix} d\varphi \\ &= \phi(0) + C_s^n \int_o^{\omega t} \begin{bmatrix} M_{xz}\cos\varphi - M_{yz}\sin\varphi \\ M_{xz}\sin\varphi + M_{yz}\cos\varphi \\ S_z \end{bmatrix} d\varphi \\ &= \phi(0) + C_s^n \begin{bmatrix} M_{xz}\sin\omega t + M_{yz}\cos\omega t - M_{yz} \\ -M_{xz}\cos\omega t + M_{yz}\sin\omega t + M_{xz} \\ S_z \omega t \end{bmatrix}.\end{aligned} \tag{A.3}$$

Deduction of equation (8): the velocity error accumulated with time can be written as the integral of equation (7):

$$\begin{aligned}\delta v_x(t) &= \delta v_x(0) + \int_0^t \left(\delta f_x - g\phi_y\right) dt, \\ \delta v_y(t) &= \delta v_y(0) + \int_0^t \left(\delta f_y + g\phi_x\right) dt.\end{aligned} \tag{A.4}$$

Normally, accelerometer error δf can be modulated by 2π rotation under stationary base. Thus, the simplified velocity model can be approximately written as

$$\begin{aligned}\delta v_x(t) &= \delta v_x(0) - g\int_0^t \phi_y dt, \\ \delta v_y(t) &= \delta v_y(0) + g\int_0^t \phi_x dt.\end{aligned} \tag{A.5}$$

Combining with equation (7), equation (A.5) can be expressed as

$$\begin{aligned}\delta v_x(t) &= \delta v_x(0) - g\int_0^t \phi_y dt \\ &= \delta v_x(0) - g\int_0^t \Big(\phi_y(0) + C_s^n(2,1) \\ &\quad \cdot \left(M_{xz}\sin\omega t + M_{yz}\cos\omega t - M_{yz}\right) \\ &\quad + C_s^n(2,2)\left(-M_{xz}\cos\omega t + M_{yz}\sin\omega t + M_{xz}\right) \\ &\quad + C_s^n(2,3) S_z \omega t\Big) dt \\ &= \delta v_x(0) - g\phi_y(0)t - C_s^n(2,1)g \\ &\quad \cdot \left(\frac{-M_{xz}\cos\omega t}{\omega} + \frac{M_{xz}}{\omega} + \frac{M_{yz}\sin\omega t}{\omega} - M_{yz}t\right) \\ &\quad - C_s^n(2,2)g\left(\frac{-M_{xz}\sin\omega t}{\omega} + \frac{M_{yz}}{\omega} - \frac{M_{yz}\cos\omega t}{\omega}\right. \\ &\quad \left. + M_{xz}t\right) - C_s^n(2,3)\frac{g}{2}S_z\omega t^2 \\ &= \Big(\delta v_x(0) - C_s^n(2,1)\frac{g}{\omega}\Big(-M_{xz}\cos\omega t + M_{yz}\sin\omega t \\ &\quad + M_{xz}\Big) + C_s^n(2,2)\frac{g}{\omega}\Big(M_{xz}\sin\omega t + M_{yz}\cos\omega t \\ &\quad - M_{yz}\Big)\Big) + \Big(-g\phi_y(0)t + C_s^n(2,1)gM_{yz}t \\ &\quad - C_s^n(2,2)gM_{xz}t - C_s^n(2,3)\frac{g}{2}S_z\omega t^2\Big).\end{aligned} \tag{A.6}$$

Similarly, the error velocity $\delta v_y(t)$ can be expressed as

$$\begin{aligned}\delta v_y(t) &= \delta v_y(0) + \int_0^t \left(\delta f_y + g\phi_x\right) dt \\ &= \Big(\delta v_y(0) + C_s^n(1,1)\frac{g}{\omega}\Big(-M_{xz}\cos\omega t + M_{yz}\sin\omega t \\ &\quad + M_{xz}\Big) - C_s^n(1,2)\frac{g}{\omega}\Big(M_{xz}\sin\omega t + M_{yz}\cos\omega t \\ &\quad - M_{yz}\Big)\Big) + \Big(g\phi_x(0)t - C_s^n(1,1)gM_{yz}t \\ &\quad + C_s^n(1,2)gM_{xz}t + C_s^n(1,3)\frac{g}{2}S_z\omega t^2\Big).\end{aligned} \tag{A.7}$$

Data Availability

Due to project team constraints, other data materials cannot be provided for the time being.

Conflicts of Interest

The authors declare that they have no conflicts of interest.

References

[1] J. D. Watson and F. H. C. Crick, "Molecular structure of nucleic acids: a structure for deoxyribose nucleic acid," *Nature*, vol. 171, no. 4356, pp. 737-738, 1953.

[2] E. Foxlin, "Pedestrian tracking with shoe-mounted inertial sensors," *IEEE Computer Graphics and Applications*, vol. 25, no. 6, pp. 38–46, 2005.

[3] J. Prieto, S. Mazuelas, and M. Z. Win, "Context-aided inertial navigation via belief condensation," *IEEE Transactions on Signal Processing*, vol. 64, no. 12, pp. 3250–3261, 2016.

[4] D. H. Titterton and J. L. Weston, "Strapdown inertial navigation technology," *Aerospace & Electronic Systems Magazine IEEE*, vol. 20, no. 7, pp. 33-34, 2004.

[5] S. Mazuelas, Y. Yuan Shen, and M. Z. Win, "Belief condensation filtering," *IEEE Transactions on Signal Processing*, vol. 61, no. 18, pp. 4403–4415, 2013.

[6] Y. Bar-Shalom, T. Kirubarajan, and X. R. Li, *Estimation with Applications to Tracking and Navigation: Theory, Algorithms and Software*, John Wiley & Sons, Hoboken, NJ, USA, 2001.

[7] E. S. Geller, "Inertial system platform rotation," *IEEE Transactions on Aerospace and Electronic Systems*, vol. AES-4, no. 4, pp. 557–568, 1968.

[8] P. Lv, J. Lai, J. Liu, and M. Nie, "The compensation effects of gyros' stochastic errors in a rotational inertial navigation system," *Journal of Navigation*, vol. 67, no. 6, pp. 1069–1088, 2014.

[9] W. Gao, Y. Zhang, and J. Wang, "Research on initial alignment and self-calibration of rotary strapdown inertial navigation systems," *Sensors*, vol. 15, no. 2, pp. 3154–3171, 2015.

[10] Q. Ren, B. Wang, Z. Deng, and M. Fu, "A multi-position self-calibration method for dual-axis rotational inertial navigation system," *Sensors and Actuators A: Physical*, vol. 219, pp. 24–31, 2014.

[11] F. Yu and S. S. Yuan, "Dual-axis rotating scheme for fiber strap-down inertial navigation system," *Journal of Harbin Engineering University*, vol. 35, no. 12, pp. 1–7, 2014.

[12] F. Sun and Y. Q. Wang, "Rotation scheme design for modulated SINS with three rotating axes," *Chinese Journal of Scientific Instrument*, vol. 34, no. 1, pp. 65–72, 2013.

[13] B. Yuan, D. Liao, and S. Han, "Error compensation of an optical gyro INS by multi-axis rotation," *Measurement Science and Technology*, vol. 23, no. 2, Article ID 025102, 2012.

[14] Q. Zhang, L. Wang, Z. Liu, and P. Feng, "An accurate calibration method based on velocity in a rotational inertial navigation system," *Sensors*, vol. 15, no. 8, pp. 18443–18458, 2015.

[15] P. Gao, K. Li, L. Wang, and Z. Liu, "A self-calibration method for accelerometer nonlinearity errors in triaxis rotational inertial navigation system," *IEEE Transactions on Instrumentation and Measurement*, vol. 66, no. 2, pp. 243–253, 2017.

[16] T. Song, K. Li, and J. Sui, "Zengjun Liu and Juncheng Liu "Self-calibration method of inner lever-arm parameters for tri-axis RINS," *Measurement Science and Technology*, vol. 28, no. 11, Article ID 115105, 2017.

[17] P. Gao, K. Li, L. Wang, and Z. Liu, "A self-calibration method for tri-axis rotational inertial navigation system," *Measurement Science and Technology*, vol. 27, no. 11, Article ID 115009, 2016.

[18] P. Gao, K. Li, L. Wang, and J. Gao, "A self-calibration method for non-orthogonal angles of gimbals in tri-axis rotational inertial navigation system," *IEEE Sensors Journal*, vol. 16, no. 24, pp. 8998–9005, 2016.

[19] S. Shang, Z. Deng, M. Fu, R. Wang, and F. Mo, "Analysis of single-axial rotation modulation influence on FOG INS precision," in *Proceedings of the 29th Chinese Control Conference*, IEEE, Beijing, China, July 2010.

[20] X. D. Yu, X. Wei, Y. Li, and X. Long, "Application of radial basis function network for identification of axial RLG drifts in single-axis rotation inertial navigation system," *Journal of National University of Defense Technology*, vol. 34, no. 3, pp. 48–52, 2012.

[21] J. Hu, X. H. Cheng, and Y. X. Zhu, "Calibration method for axial gyro drifts of single-axis rotary SINS," *Systems Engineering and Electronic*, vol. 39, no. 7, pp. 1564–1569, 2017.

[22] W. Lei, "Identification of axial RLG drift in single-axis inertial navigation system based on artificial fish swarm algorithm," *Journal of Applied Optics*, vol. 35, no. 4, pp. 725–728, 2014.

[23] L. C. Wang, K. Li, L. Wang, and J. X. Gao, "Identifying *Z*-axis gyro drift and scale factor error using azimuth measurement in fiber optic gyroscope single-axis rotation inertial navigation system," *Optical Engineering*, vol. 56, no. 2, Article ID 024102, 2017.

[24] F. Sun, J. Z. Xia, B. Y. Yang et al., "Four-position drift measurement of SINS based on single-axis rotation," in *Proceedings of the 2012 IEEE/ION Position, Location and Navigation Symposium (PLANS)*, IEEE, Myrtle Beach, SC, USA, April 2012.

[25] H. L. Yin, G. Yang, N. Song, and L. Wang, "Error propagating characteristic analyzing for rotating LG INS," *Journal of Beijing University of Aeronautics and Astronautics*, vol. 38, no. 3, pp. 345–350, 2012.

[26] B. L. Yuan, G. Y. Rao, and D. Liao, "Scale factor error analysis for rotating inertial navigation system," *Journal of Chinese Inertial Technology*, vol. 18, no. 2, pp. 160–164, 2010.

[27] F. Sun, Y. L. Chai, Y. Y. Ben, and W. Gao, "Azimuth rotation experiment and analysis for fiber-optic gyroscope strapdown system," in *Proceedings of the 2009 International Conference on Information Technology and Computer Science*, pp. 141–144, IEEE, Kiev, Ukraine, July 2009.